SURFACE DEFORMATION MONITORING ALONG QINGHAI-TIBET RAILWAY USING SMALL BASELINE SAR INTERFEROMETRY, A CASE STUDY OF BEILUHE SECTION, QINGHAI, CHINA

Fulong Chen*[1] and Hui Lin[2]

[1] Research Associate, Institute of Space and Earth Information Science, The Chinese University of Hong Kong, ShaTin, N.T., Hong Kong, China; Tel:+852-31634404;
E-mail: chenfulong@cuhk.edu.hk

[2] Professor, Department of Geography & Resource Management, The Chinese University of Hong Kong, ShaTin, N.T., Hong Kong, China; Tel: +852-26096010;
E-mail: huilin@cuhk.edu.hk

KEY WORDS: Small Baseline, SAR Interferometry, Qinghai-Tibet Railway, Surface Deformation

ABSTRACT: The project of Qinghai-Tibet Railway (QTR) confronts the challenge of surface displacements resulted from seasonal freezing bulge, thawing subsidence and compression settlement. Therefore the embankment instability monitoring is essential for policy makers as well as emergency managers for its operational safety. In this study, we implemented SAR interferometry for extracting ground deformations along the railway. In total, 38 Envisat ASAR SLC images, spanning from 18 Nov. 2004 to 17 Dec. 2009, were employed to cover the Beiluhe experimental site, Qinghai, China. Based on the small baseline interferometric combination (smaller than 300 m spatially and 175 days temporally), 49 high coherent interferograms were firstly generated to minimize the seasonal decorrelation. Then, the estimated surface deformation rates were compared between stacking and Persistent Scatterers Interferometry (PSI); the result revealed a good agreement with determination coefficient of 0.863 for a linear regression model. Furthermore, the derived deformation rates along the embankment were distinct (-20 to +20 mm/yr) in 5 years, implying the necessity of continued satellite-based surveillance along the QTR.

1. INTRODUCTION

The Qinghai-Tibet Railway (QTR) is the highest (elevation is greater than 4000 m, occasionally above 5000 m) and longest (it originates from Golmud to Lhasa with 1142 km) plateau railway in the world. It runs through about 632 km permafrost regions, including 275 km warn zones and 221 km rich ice content zone (Yu et al., 2008; Ling et al., 2010). Permafrost is a sensitive indicator of global warning. Inheritably, physical and engineering properties of permafrost are unstable and subject to temperature change. Since the construction of QTR in 2001, the regional environmental geological condition as well as moisture-heat exchange process with frozen soil has greatly changed (Li et al., 2009). The embankment of the railway confronts the challenge of surface deformation primarily controlled by seasonal freezing bulge, thawing subsidence and compression settlement. Furthermore, Qinghai-Tibet Plateau (QTP) is one of the most tectonically active areas in the world (Wang et al. 2009). Earthquakes and other tectonically motions probably cause damages to infrastructure projects in the QTP, e.g. QTR. Therefore, in order to avoid severe consequence, it is crucial to monitor the ground deformations along the QTR for its safety operation and sustainable maintenance.

Up to now, the embankment deformation and its disaster forecasts in permafrost have been well investigated by some empirical or semi-empirical formulae (Liu et al, 2002; Zhang 2004), in-situ observations (Li et al. 2006; Zhang et al., 2010a) and mechanical models (Wang et al. 2006; Mao et al., 2006). However, large-scale ground deformation monitoring is still inadequate. Moreover, as we known, the QTR is located in a rigorous and remote plateau of China; it is difficult and costly to conduct the point-based geodetic measurements (e.g. spirit leveling or GPS surveys).

Compared with ground-based techniques, the spaceborne synthetic aperture radar interferometry (InSAR) is capable of providing high-resolution, large-scale surface displacement fields (Massonnet, 1993). The persistent scatterers interferometry (PSI), represented by the Permanent Scatterers (PS) method (Ferretti et al., 2003; Colesanti & Wasowski, 2006), Interferometric Point Targets Analysis (IPTA) (Werner et al., 2003; Stramondo et al., 2008; Zhao et al., 2009), Small BAseline Subsets (SBAS) (Lanari et al., 2004; Tizzani et al., 2007), Coherent Target methods (Mora et al., 2003; Chen et al., 2010; Hui et al., 2011) and Stanford Method for Persistent Scatterer (StaMPS) (Hooper, 2008), overcomes the intrinsic limitation of conventional InSAR techniques in term of temporal, geometrical decorrelation as well as atmospheric disturbances. These innovative approaches are powerful in

deformation inversion with millimeters accuracy, which can be achieved by analyzing the point targets phases extracted from time series SAR images over the same scene.

In this study, in order to mitigate the severe seasonal decorrelation, two InSAR techniques (stacking and PSI) based on small baseline strategy were introduced to estimate the surface deformation along the QTR. The Beiluhe section is selected as the experimental site primarily due to the accessibility. A time series of 38 Envisat ASAR SLC images, spanning from 18 Nov. 2004 to 17 Dec. 2009 over the study site, were used to estimate the Line-of-Sight (LOS) motion rates and the historical deformations. The cross comparison between stacking and PSI demonstrated that the derived deformation rates were in good agreement. Several inconsistencies occurred on low coherence regions, probably due to the errors from phase unwrapping, residual height and atmospheric disturbances. InSAR technique is promising for the deformation monitoring along the embankment of QTR, validated by the ground-based leveling measurements in our study.

2. STUDY SITE AND DATA

2.1 Study Site

The QTR, a large-scale man-made linear feature, confronts irregular surface displacements owing to complicated geological and environmental conditions. Preliminary InSAR studies conducted by Chen et al. (2010) and Xie et al. (2010) indicate that the temporal decorrelation is evident primarily controlled by seasonal freezing bulge and thawing subsidence. For easily accessibility, the Beiluhe section, Qinghai, China was selected as the study site, as illustrated in Figure 1. From the SAR amplitude image, it is clear that the railway runs from south to north, demonstrating strong backscattering compared with other surrounding features (especially in northern flat terrain regions). The spatial extent of the experimental site is approximately 25×50 km^2 with upland in the south represented by Fenghuo Mount and mild terrain in the north represented by Beiluhe valley. The arid continental climates are prevailing here because of the high elevation varying from 4500 m to 5200 m. The freezing period usually lasts from September to April of next year (7~8 months) and the mean annual air temperature is about -3.8℃. The averaged permafrost table is about 2.0 m and the mean annual ground temperature ranges from -0.8 to -1.0℃. Warm and ice-rich permafrost is well developed here with ground ice of 2.0~8.0 m depth under the natural ground surface (Zhang et al., 2010a). The past field investigations indicate four main features, including rocky mountain, alpine meadow, water body and the railway (see Figure 1).

The QTR project is a 100-year grand plan for generations to come; therefore its embankment instability needs to be well monitored. Plentiful studies, including “roadbed cooling” approaches (Yu et al., 2008), engineering geology and frozen soil analysis (Ling et al., 2010), seismic analysis (Li et al, 2009) as well as wind-blown sand influences (Zhang et al., 2010b), have been conducted. Besides commonly interesting effects, the embankment deformation monitoring is also covered by recent preliminary studies (Li et al. 2009; Zheng et al. 2010). Xie et al. (2010) tried to use PSI to detect the large-scale deformations over permafrost region of QTP, offering promise for the deformation extraction using InSAR techniques along the QTR.

2.2 Data

Totally 38 Envisat ASAR images, descending with mode of image swath 2, acquired from Nov. 2004 to Dec. 2009, were used in this study, as listed in Table 1. Those data were provided under the European Space Agency (ESA)-National Remote Sensing Center of China (NRSCC) Dragon cooperation project. The pixel spacing is 3.90 m in the range direction, and 4.05 m in the azimuth direction. A subset of approximately 25×50 km^2 over Beiluhe section was cropped from the original images (Figure 1). DORIS precise orbits data provided by the ESRIN Help desk of ESA were applied to calculate interferometric baselines. The 3-arcsecond (~90 m) Shuttle Radar Topography Mission (SRTM) DEM data from the United States Geological Survey (USGS) were used for topographic phase estimation at first step, and then for geocoding (transforming Range-Doppler coordinates into Universal Transverse Mercator map geometry system). Ground-based leveling data in the span of Oct. 2005 to Dec. 2009 were available for the validation of InSAR-derived results, as marked by the cross symbol in Figure 1.

3. METHODOLOGY AND DATA PROCESSING

Because of the complicated scenarios in the QTP, previous studies demonstrated the challenge and potential of InSAR techniques to detect surface displacement in the permafrost regions (Xie et al., 2010; Chen et al., 2010). The primary limitations of InSAR techniques in the experimental site are the severe temporal decorrelation and non-linear motion trends by seasonal alternation. Moreover, the results could be influenced by atmospheric disturbances as well (Hanssen, 2001; Zebker et al., 1997). Therefore in this study, stacking and PSI based on small baseline strategy were employed for deformation trends inversion to conquer above limitations.

Table 1. Envisat ASAR Data Used In This Study. The Image Of 20070726 Was Chosen As The Reference For Image Coregistration To Minimize The Distance Of Available SAR Acquisitions In The Domain Of Geometric-temporal Baselines.

Acquisition data (yymmdd)	Perpendicular baseline (meters)	Temporal baseline (days)
20041118	-79.0342	-980
20041223	-15.4134	-945
20050127	0.3222	-910
20050303	125.1759	-875
20050407	-184.838	-840
20050721	701.5827	-735
20050929	-48.3777	-665
20060216	-224.312	-525
20060323	320.1585	-490
20060427	239.7703	-455
20060601	-797.66	-420
20060706	936.1837	-385
20060914	-804.843	-315
20061019	-324.962	-280
20061228	470.4177	-210
20070412	-159.574	-105
20070517	-129.439	-70
20070621	63.8025	-35
20070726	0	0
20070830	209.4565	35
20071004	-83.7819	70
20071108	194.5151	105
20071213	-249.584	140
20080221	-301.909	210
20080501	-80.907	280
20080605	154.0245	315
20080918	-244.248	420
20081023	239.0536	455
20090101	154.7455	525
20090205	-269.455	560
20090312	510.3546	595
20090416	-196.656	630
20090521	-13.4559	665
20090625	344.1177	700
20090730	-8.6156	735
20090903	295.0974	770
20091008	-84.0877	805
20091217	-278.472	875

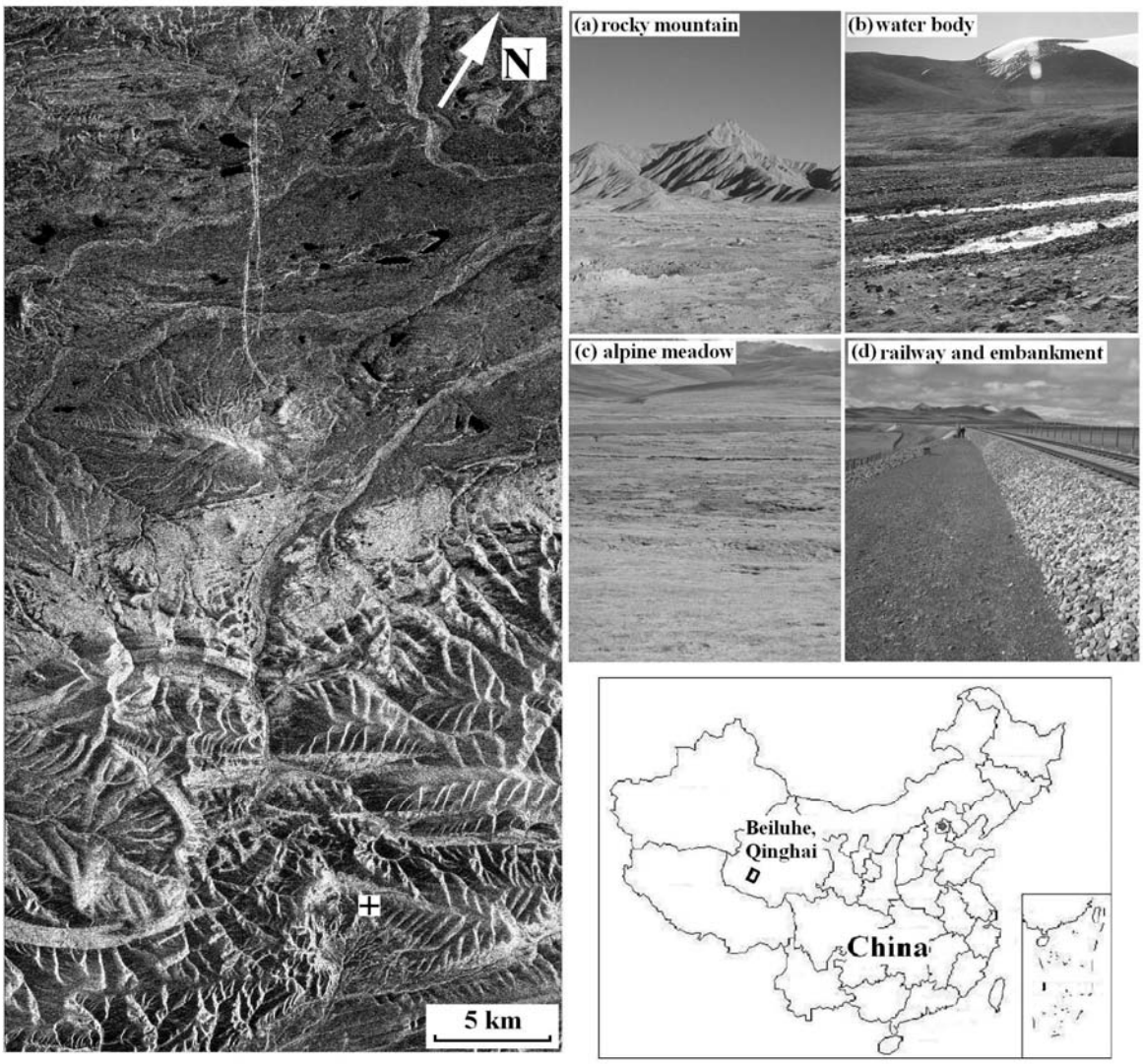

Figure 1. Study Site Of Beiluhe Section, Qinghai, China. Four Main Features Were Prevailing In This Area, Rocky Mountain, Water Body, Alpine Meadow, Embankment Of The Railway. The Cross Symbol Indicates The Location Of Available Leveling Data.

3.1 Interferogram Generation

The choice of the data pairs was stipulated, and the small baselines (smaller than 300 m spatially and 175 days temporally) resulted in high coherence, which was required by interferogram phase unwrapping. Another decorrelation factor was the Doppler centroid; the differences below 100 Hz were selected for interferometric analysis. Using those thresholds, 49 interfergrams were firstly generated. Then, the precise DORIS orbit vectors were used for flat earth phase estimation, and the SRTM DEM data were employed for topographic phase simulation. After that, the differential interferograms were derived by subtracting the flat earth and topographic phase components from the original interferograms.

3.2 Stacking

Stacking is the advance of conventional differential InSAR technique. It can be used to estimate the linear deformation rate using a set of unwrapped differential interferograms. Therefore, the 49 differential interferograms were unwrapped in advance using a minimum cost-flow (MCF) and triangulation method (Costantini 1998). The individual interferogram phases are weighted by the time interval to estimate the deformation rate based on the assumption that atmospheric statistics are stationary among temporal epochs. Providing there are N available interferograms, the deformation signal phase can be enhanced by N times, but only $\sqrt{N}$ larger for the atmospheric phase noise, and thus the signal to noise ratio can be increased by a factor of $\sqrt{N}$ (Biggs et al., 2007; Strozzi et al., 2001). The estimate of the mean deformation rate using stacking at each location of interferograms is presented as

follows:

$$\begin{cases} ph\_rate = Sum(w_i * p_i) \\ w_i = delta\_T_i^2 \end{cases} \quad (1)$$

Where p_i is the ith interferogram phases, w_i is the weight determined by time intervals $delta\_T$ of interferometric image pairs.

3.3 PSI

One of the PSI approaches referred to IPTA was introduced in this study. This technique is capable of reducing the errors resulting from the atmospheric path delay and increasing the temporal sampling rate by analyzing the extracted point-like targets or so-called Persistent Scatterers (PSs). The initial PS candidates were determined by two selection criteria. One was based on the low temporal backscatter variability of co-registered SLC stacks, and the other was derived by utilizing the spectral properties of each individual SLC data. The unwrapped interferometric phase model ϕ_{unw} in IPTA is the sum of topographic phase ϕ_{topo}, ground deformation phase ϕ_{def}, differential atmospheric phase ϕ_{atm} and phase noise ϕ_{noise}:

$$\phi_{unw} = \phi_{topo} + \phi_{def} + \phi_{atm} + \phi_{noise} \quad (2)$$

Generally, in IPTA analysis a two-dimensional linear regression is firstly applied on the baseline and acquisition time interval domain to estimate the residual height and linear deformation rate (Jiang et al., 2011). For large stacks of SAR images and a small phase gradient, the two-dimensional regression can find the correct phase ambiguities (Wegmuller et al., 2004), otherwise the phase unwrapping needs to be performed before the regression. In this investigation, the phase unwrapping was performed in the spatial domain using the MCF algorithm for sparse point data (Costantini & Rosen, 1999). Then, the atmospheric phase, non-linear deformation and error terms of the residual phase could be further discriminated utilizing their different spatial and temporal dependencies. The significant advantage of the IPTA technique is the possibility of a step-wise, iteration improvement during the model parameters calculation. The final results consist of linear deformation rates, height corrections, atmospheric phases, refined orbits as well as historical displacement time series for each qualified PS point. The derived accuracy of deformation rate is in the order of 1~2 mm/yr (Teatini et al., 2005; Stramondo et al., 2008), however, the evaluation of results also depends on the specific data used, processing and observed scenarios.

4. RESULTS AND VALIDATION

4.1 Results

The average LOS displacement rates over the Beiluhe section by stacking were illustrated in Figure 2, with values ranging from -20 mm/yr to 20 mm/yr in the span of Nov. 2004 to Dec. 2009. The negative sign of the deformation rates stands for an increasing distance with time away from the satellite (subsidence); and positive sign represents uplift motion. Referring to the terrain (Figure 1), we found that the subsidence regions were primarily located in flat regions or steam valleys. The intersection of flat terrains and WIRP regions implies that the surface subsidence occurred on WIRP sites from the permafrost thawing. In contrast, subtle-medium uplift occurred on hilly mountains because of freezing bulge where temperature was rather low. The marked white line (Figure 2) indicated the location of QTR and its corresponding embankment. From Figure 2, it is clear that the deformation trend was uneven along the embankment of the railway. The railway ran across two typical WIRP regions, Beiluhe valley “A” and Fenghuo Mount valley “B” (Figure 2), demonstrating as obvious subsidence. The mild uplifts were primarily located in the embankment regions with proactive “cooling down” measures (Yu et al., 2008).

The PSI-derived ground deformation rates were illustrated in Figure 3. A large number of PS points were detected within the study area (average density of 45 PS/km2), although the seasonal decorrelation was evident. A mass of PSs were extracted along the railway (white line in Figure 3), particularly when the embankment direction was approximately parallel to the path of the satellite. The PS points in the southern and north-eastern were relative sparse. Low PS density in Fenghuo Mount (southern part) probably results from decorrelation of seasonal snow cover. For the Beiluhe valley (north-eastern part), the terrain of sand land cover is smooth, resulting in lack of PS targets. The displacement rates derived by PSI were also in the range of -20 mm/yr to 20 mm/yr in the 5-year observation span. Two subsidence regions (“A” and “B”), Beiluhe and Fenghuo Mount valleys, were evident along the railway, coincided with the stacking results.

4.2 Comparison and Validation

A preliminary cross comparison was conducted between the stacking and PSI derived results. The deformation patterns from these two techniques were quite similar; not only the deformation ranges but also the location of subsidence zones (see Figure 2 and 3). However, several inconsistent regions occurred. The disagreements can be interpreted from three aspects. The first cause is phase unwrapping error, which can occur in low coherent regions for stacking and low density PS regions for PSI. The second one is residual height phase errors. In general, PSI is capable of estimating deformation rates and residual height simultaneously; however for stacking technique, only velocity estimation is achievable. The last fact is atmospheric artifacts. For PSI technique, the atmospheric delay can be eliminated by spatial-temporal filters; but for stacking, the disturbances can only be mitigated with a factor of $\sqrt{N}$.

Then, we extracted deformation values at 13 sampling points along the embankment. The values comparison between stacking and PSI was illustrated in Figure 4. The deformation discrepancy along the embankment was much smaller compared to surrounding regions, demonstrating a good agreement represented by the linear fit model $y = 0.8121x - 2.4984$ with determination coefficient of 0.863. The bias of deformation values between stacking and PSI was 1~8 mm/yr, once more, revealing consistency of derived results.

As a further validation, the accumulative deformations from PSI and leveling measurements were compared. The leveling measurement campaign was designed for embankment deformation monitoring of QTR. The historical displacements of a point (nearby Fenghuo Mount Tunnel) with one month interval were available, as marked by the cross in Figure 1. They were collected from Oct. 2005 to Dec. 2009. The accumulative deformation of leveling data during the observation period was 13 mm. For the PSI, the accumulative deformation can be calculated from the motion time series, and the corresponding value was 15 mm. The good agreement demonstrated that the PSI-derived results were reliable.

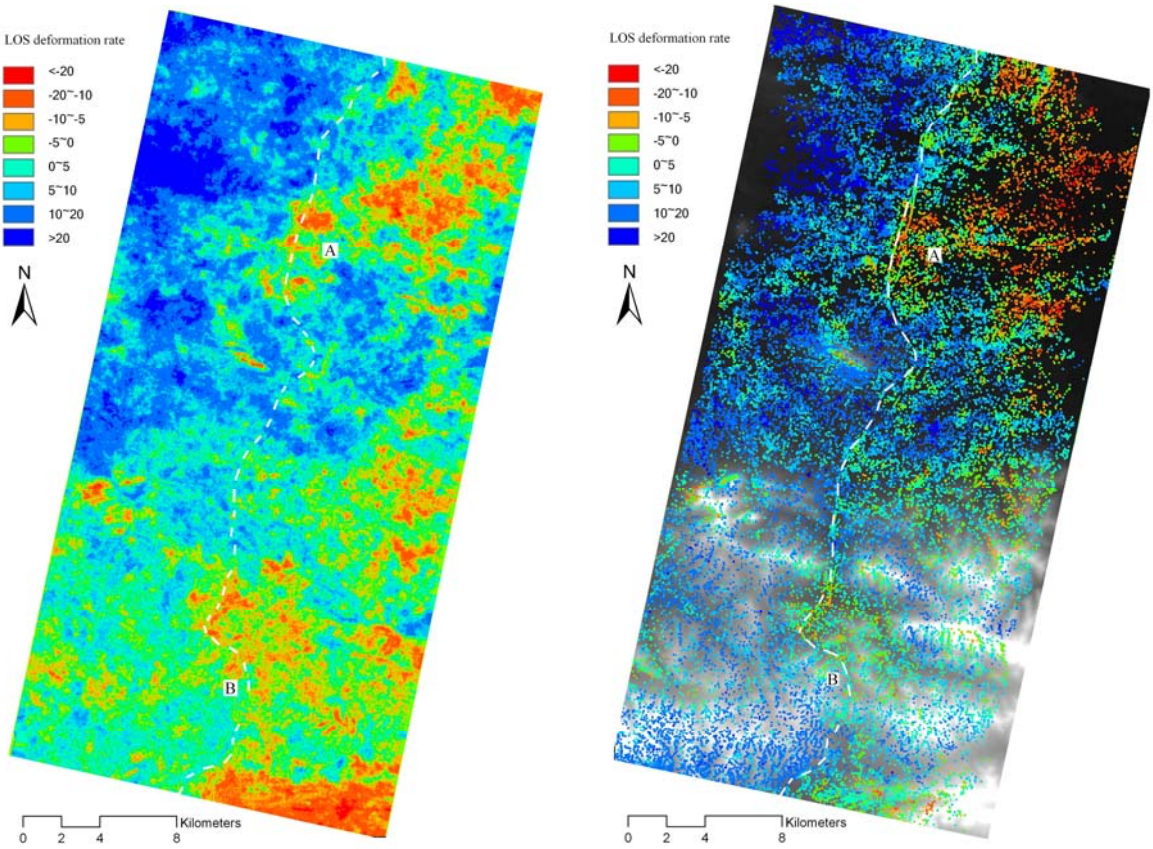

Figure 2 Deformation Rates Over Beiluhe Section Derived By Stacking Differential InSAR Technique; “A” And “B” Are Two WIRP Regions With Obvious Subsidence.

Figure 3 Deformation Rates Over Beiluhe Section Derived By PSI Technique, Indicating Similar Motion Patterns Of Stacking. “A” And “B” Are Two WIRP Regions With Obvious Subsidence.

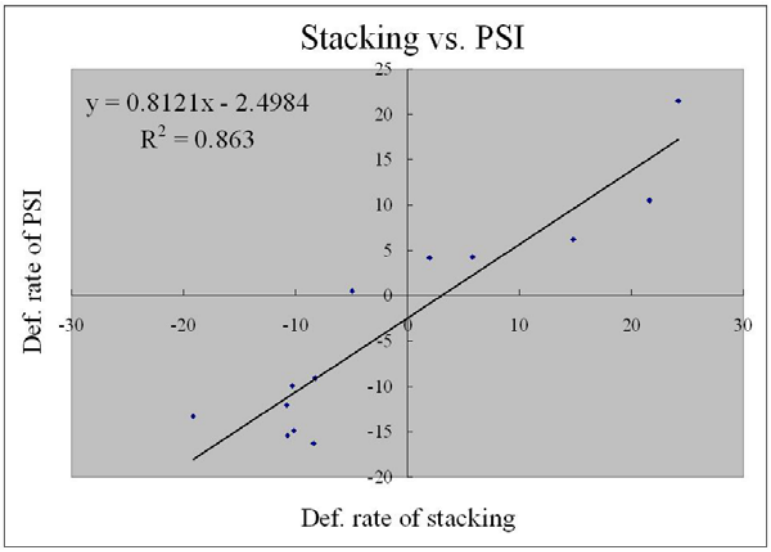

Figure 4. Deformation Rates Comparison Between Stacking And PSI. A Good Agreement Is Represented By The Linear Polynomial Fit Expression $y = 0.8121x - 2.4984$ With Determination Coefficient $R^2 = 0.863$.

5. DISCUSSION

The complementary use of stacking and PSI provides capability for a better detection of the surface deformation in the Beiluhe section study site. In general, PSI allows the retrieval of deformation time series as well as more precise velocity estimation than stacking technique. However, PSI is limited to regions with low density of PS points due to high deformation gradient or low coherence. In contrast, stacking is possible to detect the surface deformations over the whole scene, although the accuracy is weaker than PSI due to the atmospheric artifacts and topographic height errors. Generally, the displacement mechanism of permafrost is rather complex. Compared with C-band Envisat ASAR data, L-band ALOS PALSAR has a longer wavelength and better coherence, and thus offers promise for extraction deformations in case of high deformation gradient (Sandwell et al., 2008), e.g. in QTR site. In addition, characterized by higher space resolution, revisit frequency and precise geometric locating (Eineder et al., 2009), the newly-launched spaceborne SAR systems (e.g. TerraSAR-X and COSMO-SkyMed) also enhance the detection capability for more detailed, complex motions, e.g. severe seasonal trends in QTP.

Noting that the surface deformation along the QTR can lead to not only vertical motion but also lateral movements (e.g. tectonically motion). InSAR products can basically measure the LOS deformations if only one orbit direction (e.g. ascending or descending) is used. In other words, the InSAR-derived results are more sensitive to vertical motion than other directions because of the small incidence angle of Enivsat ASAR data (Jiang et al., 2011). Thereby, for a through understanding of surface displacement behaviors, a multiple-pass InSAR for 3D deformation map retrieval has to be considered. Furthermore, a synergistic analysis of InSAR, empirical models and in-situ measurements (precise leveling, GPS and kinematic observations) is another feasible approach.

6. CONCLUSION

In this investigation, we applied InSAR approaches, including stacking and PSI, to detect the surface deformation along the QTR. The interferometric decorrelation was mitigated owing to the small baseline strategy. Surface motions in Beiluhe section, Qinghai, China were estimated using 38 Envisat ASAR images in the span of 5 years. The cross comparison of both InSAR approaches demonstrated good agreement. Then, the measurements from ground-based leveling measurements and PSI were compared; the coherent relationship implied the reliability of PSI-derived results. This study demonstrated the promise of InSAR techniques for permafrost deformation monitoring. However, it is worth remarking that interferometric decorrelation due to seasonal rapid displacement is still a challenge for the InSAR monitoring in permafrost region (e.g. QTP). The problem could cause phase unwrapping which results in deformation inconsistency in stacking and PSI results (see Figure 2 and 3). For the purpose of reliability improvement, our further studies will focus on the embankment instability monitoring of QTR using L-band ALOS PALSAR together with new generation of TerraSAR-X or COSMO-SkyMed data, which would offer meaningful counter-measures in the face of potential geological hazards.

Acknowledgments

This study has been supported by funding from the Research Grants Council of HKSAR, China (CUHK450210) and a Direct Grant of the Chinese University of Hong Kong (2021029). The digital elevation model of the investigated zone was acquired through the SRTM archive. The Envisat ASAR data over QTR study site have been provided under the ESA-NRSCC Dragon cooperation project. We also thank Prof. Guo Jianwen from Cold and Arid Regions Environmental and Engineering Research Institute, Chinese Academy of Sciences for providing the ground-based leveling data.

References

[1]Biggs, J., Wright, T., Lu, Z., & Parsons, B., 2007. Multi-interferogram method formeasuring interseismic deformation: Denali Fault, Alaska. Geophysical Journal International, 170, pp.1165−1179.

[2]Chen F. L., Lin H., Li Z., et al., 2010. Qinghai-Tibet railway displacement monitoring using ALOS PALSAR differential SAR interferometry. in International Workshop on Spatial Information Technologies for Monitoring the Deformation of Large-Scale Man-made Linear Features, Jan. 11-12, Hong Kong, China (CDROM)

[3]Chen F, Lin H., Yeung K. and Cheng S., 2010. Detection of slope instability in Hong Kong based on multi-baseline differential SAR interferometry using ALOS PALSAR data. GIScience and Remote Sensing, 47(2), pp. 208-220.

[4]Colesanti C., & Wasowski, J., 2006. Investigating landslides with spaceborne Synthetic Aperture Radar (SAR) interferometry. Engineering Geology, 88, pp.173-199.

[5]Costantini M., 1998. A novel phase unwrapping method based on network programming. IEEE Transactions on Geoscience and Remote Sensing, 36, pp. 813-821.

[6]Costantini M., & Rosen P., 1999. A generalized phase unwrapping approach for sparse data. in Proceeding of International Geoscience and Remote Sensing Symposium 1999 (IGARSS 1999), Hamburg, Germany, June 28-July 2. Vol 1, pp. 267-269.

[7]Eineder, M., Adam, N., Bamler, R., Yague-Martinez, N., & Breit, H., 2009. Spaceborne spotlight SAR interferometry with TerraSAR-X. IEEE Transactions on Geoscience andRemote Sensing, 47, pp.1524−1535.

[8]Ferretti, A., Prati, C., & Rocca, F., 2000. Nonlinear subsidence rate estimation using persistent scatterers indifferential SAR interferometry. IEEE Transactions on Geoscience and Remote Sensing, 38(5), pp. 2202-2212.

[9]Hanssen, R. F., 2001. Radar Interferometry. Data Interpretation and Error Analysis, Dordrecht, Kluwer Academic Publishers, pp.138.

[10]Hooper A., 2008. A multi-temporal InSAR method incorporating both persistent scatterer and small baseline approaches. Geophysical Research Letters, 35, pp.1-5.

[11]Jiang L., H. Lin, Ma J., Kong B., and Wang Y., 2011. Potential of small-base SAR interferometry for monitoring land subsidence related to underground coal fires: Wuda (Northern China) case study. Remote Sensing of Enviroment, 115, pp. 257-268.

[12]Lanari, R., Mora, O., Manunta, M., 2004. A small-baseline approach for investigating deformations on full-resolution differential SAR interferograms. IEEE Transactions on Geoscience and Remote Sensing, 42(7), pp. 1377-1386.

[13]Li S., Lai Y., Zhang M. & Dong Y., 2009. Study on long-term stability of Qinghai-Tibet Railway embankment. Cold Regions Science and Technology, 57, pp.139-147.

[14]Li Z., Xu W., Chen M., 2006. Settlement characteristics of Qinghai-Tibetan railway embankemnt on permafrost subgrade in Qingshui river region of Tibet plateau, China. Journal of Engineering Geology, 14, pp.824-829.

[15]Lin H., Chen F., Zhao Q., 2011. Land deformation monitoring using coherent target-neighborhood networking method combined with polarimetric information——a case study of Shanghai, China. International Journal of Remote Sensing, 32, pp.2395-2407.

[16]Ling X., Chen S., Zhu Z., Zhang F., Wang L. & Zou Z., 2010. Field monitoring on the train-induced vibration response of track structure in the Beiluhe permaforst region along Qinghai-Tibet railway in China. Cold Regions Science and Technology, 60, pp.75-83.

[17]Liu Y., Wu Q., Zhang J. et al., 2002. Deformation of highway roadbed in permafrost regions of the Tibetan Plateau. Journal of Glaciology and Geocryology 24, pp.10-15.

[18]Mao X., Wang B., Hu. C., et al., 2006. Numerical analyses of deformation and stress fields in permafrost regions. Journal of Geocryology, 28, pp.396-400.

[19]Massonnet, D., Rossi, M., Carmona, C., Adragna, F., Peltzer, G., Feigl, K., & Rabaute, T., 1993. The displacement field of the Landers earthquake mapped by radar interferometry. Nature, 364, pp.138−142.

[20]Mora, O., Mallorqui, J. J., & Broquetas, A., 2003. Linear and nonlinear terrain deformation maps from a reduced set of interferometric SAR images. IEEE Transactions on Geoscience and Remote Sensing, 41, pp.2243−2253.

[21]Sandwell, D. T., Myer, D., Mellors, R., Shimada, M., Brooks, B., & Foster, J., 2008. Accuracy and resolution of ALOS interferometry: Vector deformation maps of the father's day intrusion at Kilauea. IEEE Transactions on

Geoscience and Remote Sensing, 46, pp.3524−3534.
[22]Stramondo S., Bozzano F., Marra F., Wegmuller U., Cinti F. R., Moro M., et al., 2008. Subsidence induced by urbanisation in the city of Rome detected by advanced InSAR technique and geotechnical investigations. Remote Sensing of Environment, 112, pp.3160−3172.
[23]Strozzi, T., Wegmuller, U., Tosi, L., Bitelli, G., & Spreckels, V., 2001. Land subsidencemonitoring with differential SAR interferometry. Photogrammetric Engineering &Remote Sensing, 67, pp.1261−1270.
[24]Teatini P., Tosi L., Strozzi T., Carbognin L., Wegmuller U., & Rizzetto F., 2005. Mapping regional land displacements in the Venice coastland by an integrated monitoring system. Remote Sensing of Environment, 98, pp.403−413.
[25]Tizzani P., Berardino P., Casu F., Euillades P., Manzo M., Ricciardi G.P., Zeni G., Lanari R., 2007. Surface deformation of Long Valley caldera and Mono Basin, California, investigated with the SBAS-InSAR approach. Remote Sensing of Enviroment 108, pp.277-289.
[26]Wang J., Huang X., Hou S., 2006. Numerical analysis of pavement deformation and stress in permafrost regions. Journal of Glaciology and Geocryology, 28, pp.217-222.
[27]Wang L., Wu Z., Sun J., Liu X., and Wang Z., 2009. Characteristics of ground motion at permafrost sites along the Qinghai-Tibet railway. Soil Dynamics and Earthquake Engineering, 29, pp.974-981.
[28]Wegmuller U., Werner C., Strozzi T. & Wiesmann A., 2004. Monitoring mining induced surface deformation. in Proceeding of International Geoscience and Remote Sensing Symposium (IGARSS 2004), 20-24, Sep. 2004, Anchorage, Alaska, USA, pp. 1933-1935.
[29]Werner, C., Wegmuller, U., & Strozzi, T., Wiesmann, A., 2003. Interferometric point target analysis for deformation mapping. in Proceeding of IEEE Geoscience and Remote Sensing Symposium (IGARSS'03), July 2003,Toulouse, France, pp. 4362-4364.
[30]Xie C. Li Z., Xu J. and Li X., 2010. Analysis of deformation over permafrost regions of Qinghai-Tibet plateau based on permanent scatterers. International Journal of Remote Sensing, 31, pp.1995-2008.
[31]Yu Q., Niu F., Pan X., Bai Y. & Zhang M., 2008. Investigation of embankment with temperature-controlled ventilation along the Qinghai-Tibet Railway. Cold Regions Science and Technology, 53, pp.193-199.
[32]Zebker, H.A., P.A. Rosen & S. Hensley,1997. Atmospheric effects in interferometric synthetic aperture radar surface deformation and topographic maps, Journal of Geophysical Research, 102(4), pp.7547-7563.
[33]Zhang B., Zhang J., and Qin Y., 2010a. Investigation for the deformation of embankment underlain by warm and ice-rich permafrost, Cold Regions Science and Technology, 60, pp.161-168.
[34]Zhang J., 2004. Study on roadbed stability in permafrost regions on Qinghai-Tibetan Plateau and classification of Permafrost in highway engineering. PhD Dissertation for Graduate University of the Chinese Academy of Sciences, Beijing, pp.35-62 (in Chinese).
[35]Zhang K., Qu J., Liao K., Niu Q. Han Q., 2010b. Damage by wind-blown sand and its control along Qinghai-Tibet Railway in China. Aeolian Research, 1, pp.143-146.
[36]Zhao, Q., Lin, H., Jiang, L., Chen, F., & Cheng, S, 2009. A study of ground deformation in Guangzhou urban area with persistent scatterer interferometry. Sensors, 9, pp.503-518.